Solar Physics
DOI: 10.1007/•••••-•••-•••-••••-•

The EVE Doppler Sensitivity and Flare Observations

H. S. Hudson[1,2], T. N. Woods[3], P. C. Chamberlin[4], L. Fletcher[2], G. Del Zanna[6], L. Didkovsky[5], N. Labrosse[2], and D. Graham[2]

Abstract The Extreme-ultraviolet Variability Experiment (EVE; see Woods et al. 2009) obtains continuous EUV spectra of the Sun viewed as a star. Its primary objective is the characterization of solar spectral irradiance, but its sensitivity and stability make it extremely interesting for observations of variability on time scales down to the limit imposed by its basic 10 s sample interval. In this paper we characterize the Doppler sensitivity of the EVE data. We find that the the 30.4 nm line of He II has a random Doppler error below 0.001 nm (1 pm, better than 10 km/s as a redshift), with ample stability to detect the orbital motion of its satellite, the *Solar Dynamics Observatory (SDO)*. Solar flares also displace the spectrum, both because of Doppler shifts and because of EVE's optical layout, which (as with a slitless spectrograph) confuses position and wavelength. As a flare develops, the line centroid also displays variations that reflect Doppler shifts and therefore flare dynamics. For the impulsive phase of the flare SOL2010-06-12, we find the line centroid to have a redshift of 16.8 ± 5.9 km/s relative to that of the flare gradual phase. We find also that high-temperature lines, such as Fe XXIV 19.2 nm, have well-determined Doppler components for major flares, with decreasing apparent blueshifts as expected from chromospheric evaporation flows.

Keywords: Sun: flares — Sun: photosphere

1. Introduction

The directly radiated energy of a solar flare represents a substantial fraction of the total energy released from the magnetic field (e.g., Emslie *et al.*, 2005).

[1]SSL, UC Berkeley, CA, USA 94720
[2]School of Physics and Astronomy, SUPA, University of Glasgow
[3]Laboratory for Atmospheric and Space Physics, University of Colorado, 1234 Innovation Dr., Boulder, CO 80303, USA
[4]NASA Goddard Space Flight Center
[5]Space Sciences Center, University of Southern California, Los Angeles, CA 90089, USA
[6]University of Cambridge

Much of this energy appears in the UV and EUV spectral ranges, because the emission results from heating. In a recent breakthrough observation, Woods et al. (2004) successfully detected a solar flare (SOL2003-10-28T11:10, X17.2) in the total solar irradiance (TSI), thus capturing an upper limit on the UV/EUV energy. Until now we have had only limited detailed characterization of the energy distribution of this component of flare emission, but with the launch of the *Solar Dynamics Observatory (SDO)* and its Extreme-ultraviolet Variability Experiment (EVE; see Woods et al. 2009) this picture has changed substantially. EVE provides broad-band and narrow-band irradiance measurements across the range 5-105 nm with 0.1 nm resolution, plus broad bands in its EUV SpectroPhotometer (ESP) experiment (Didkovsky *et al.*, 2009). The narrow-band spectra have integration times of 10 s, and the broad-band photometry 0.25 s. These properties are unprecedented for studies of solar flares.

The EVE observations have no spatial resolution, i.e. they treat the Sun as a star. In some spectral bands this means a high nonflaring background level, compared to the situation for observations of stellar flares, which typically appear on intrinsically fainter stars. The EVE spectra benefit by having excellent signal-to-noise ratio, as illustrated below, and excellent calibration. In the impulsive phase of a flare we do not yet have a good characterization of the flare spectrum owing to the poor temporal or spatial sampling of instruments such as the SO82A instrument on *Skylab* (Feldman, 1987), CDS on *SOHO* (Del Zanna *et al.*, 2006), or of EIS on *Hinode* (Del Zanna et al., 2011). The UVSP instrument on the *Solar Maximum Mission* (Woodgate *et al.*, 1980) could do rapid rastering, as good as 4.6 s cadence over a $28'' \times 28''$ field of view, or 7×7 pixels (Cheng *et al.*, 1981). We note also the Sun-as-a-star observations reported by Lemaire *et al.* (2004), who used SUMER observations of scattered radiation in the Ly continuum region to observe SOL2001-08-25T16:45 (X5.3). Likewise Raymond *et al.* (2007) used *SOHO*/UVCS to study transition-region fluxes in the flare impulsive phase, again indirectly via scattered radiation.

The EVE spectra make it possible for the first time to compare time-series and Doppler spectroscopy of solar transients on the same footing as stellar observations of essentially point sources. The EVE solar observations also have potential interest because of their precision and stability (as discussed in detail below). In addition, we have excellent imaging observations from other instruments, especially the Atmospheric Imaging Array (AIA) EUV imager; AIA is on the same spacecraft and has multiple EUV bands with a cadence of 12 s. In addition we have relatively well-developed numerical tools (e.g., Allred *et al.*, 2005) that can in principle be used to link the imaging and spectroscopic observations. Thus the solar interpretation of these Sun-as-a-star observations has several advantages over purely stellar observations. This paper describes the potential capabilities of EVE, specifically its MEGS-A component, for Doppler measurements. We focus on the 30.4 nm line of He II, which has excellent signal-to-noise ratio, but also give examples of line centroid variations at other wavelengths in flares. Our basic procedure for this paper is to fit each 10 s data accumulation in the EVE/MEGS-A Level 2 data with a single-component Gaussian line profile (six parameters for the line and a quadratic background term), as shown in Figure 1. This standard fit does not represent the 30.4 nm line exactly, as discussed below.

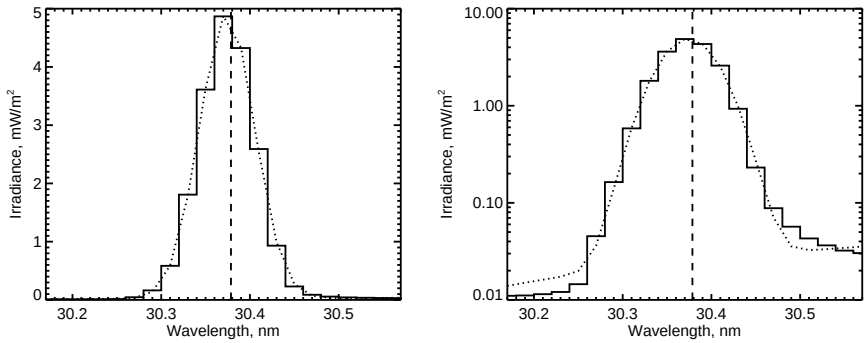

Figure 1. Linear and log representations of simple standard fits to a single EVE/MEGS-A data sample, 00:00:11.389 UT 4 January 2011. The fitting function has six parameters defining a Gaussian line component plus a quadratic background component. The fit result for line width is $\sigma = 0.0309$ nm.

2. The He II 30.4 nm line centroid

We first examine the long-term (days) variation of the 30.4 nm line. Figure 2 shows the irradiance and centroid results for a typical day of medium solar activity, 4 January 2011. These parameters come from a standard fitting function, which assumes a single Gaussian line on a quadratic background. Our fits use 21 spectral points centered on the Chianti line position. Figure 2 reveals small fluctuations around a steady level of He II irradiance, with some weak increases coinciding with *GOES* B- and C-class flares. The line centroid varies by less than one pm (less than 10 mÅ) over this day, excluding an artifact at about 15:00 UT, and the rms variation of the centroid position derived from the fits is ∼0.11 pm, as derived from the first 100 10-s data points (an interval without listed flare events). Interpreted as a redshift, this corresponds to a standard deviation $\sigma \approx 1$ km s^{-1}. The EVE spectroscopy thus has sufficient spectral resolution for relatively good measurements of line shifts, even though its primary design objective is to obtain precise irradiance measurements.

The results of the standard line fits for a longer period (Figure 3) show that the trends seen in Figure 2) consist of a regular diurnal term, reflecting the orbital motion of *SDO* in geosynchronous orbit, plus additional features. The Doppler shift of the orbital motion is approximately ±3 km s^{-1}. These latter features include systematic errors, some of which are not yet identified. The major one corresponds to the effects of a daily calibration sequence (for example, in Figure 3 at about 15:15 UT).

Many causes of centroid variation affect the results seen in Figures 2 and 3: photon counting statistics, thermal stresses within the instrument, variable line blends, line profile variations, true Doppler shifts due to both solar sources and spacecraft motions, and spatial/spectral confusion inherent in the MEGS-A optical design. The latter effect arises because the MEGS-A CCD detector is not mounted on the Rowland circle, in order to optimize the spectral resolution with a grazing-incidence spectrograph (Crotser et al., 2007; Woods et al., 2010). There

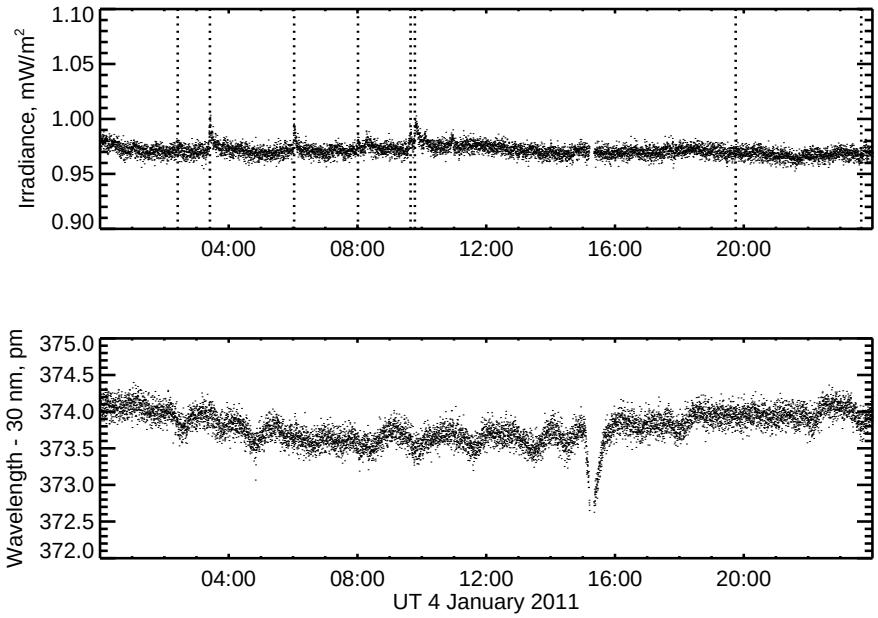

Figure 2. *Upper:* time variation of the irradiance, and *lower*, the line centroid for standard fits of the 30.4 nm line predominantly of He II, obtained for one day of quiet solar conditions. The dotted vertical lines show the times of GOES X-ray events, with SOL2011-01-04T03:33 (C1.9) the most energetic one. The feature just after 15:00 is an artifact resulting from a daily calibration operation.

is thus a relationship between the spatial position of a source and its interpreted spectral parameters, such as the centroid wavelength. We have characterized this dependence empirically from pre-launch calibrations and present these results here.

The MEGS-A spectra are recorded as dispersed slit images on a CCD (see the examples given by Crotser *et al.*, 2007). The calibration software collapses this 2D representation of the spectrum into its 1D form. The spectral image varies slightly with angle of incidence, as in a slitless spectrograph. We present here a representation of this dependence based upon pre-flight calibration data, for which the angle of incidence could be varied explicitly. For a source at heliographic angles (θ, ϕ) (EW, NS), the spectral displacement from a source at disk center is given approximately by

$$\Delta\lambda \approx 6.5\ \sin\theta - 18.5\ \sin^2\theta + 3.5\ \sin\phi \quad \text{pm}, \tag{1}$$

Thus for a source at the W limb exactly ($\theta = 90^\circ, \phi = 0^\circ$), the displacement would be -12.5 pm. The net shift for a source that is only a fraction of the total brightness of the Sun is proportionally smaller. The data have sufficient precision to permit an in-flight calibration of this function based on independent knowledge of flare locations, after sufficient data have been accumulated, and so the result in Equation 1 should be regarded as tentative. Note that this dis-

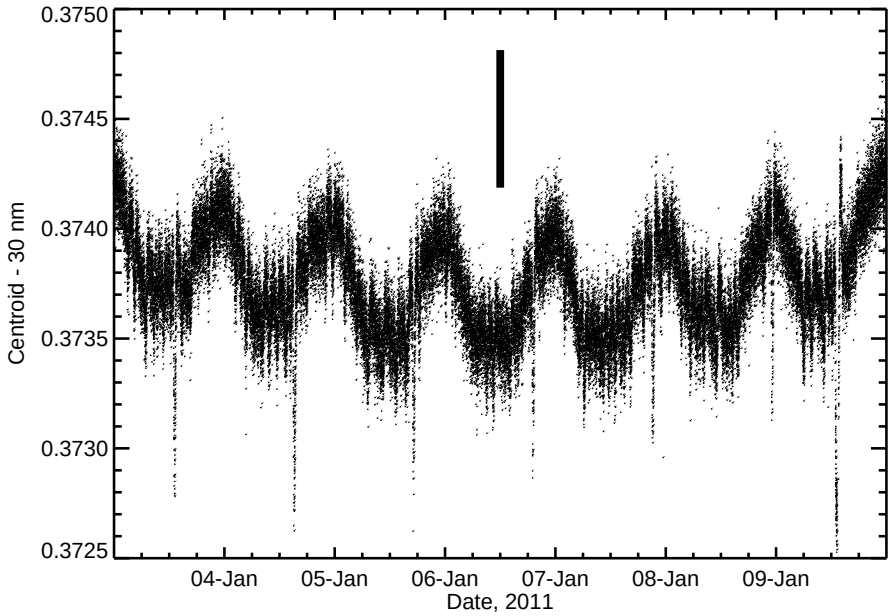

Figure 3. Variation of 30.4 nm line centroid as a function of time across one week of solar quiet conditions, expressed as a Doppler shift for fits to single 10 s integrations. Although many artifacts appear in the data, the orbital motion of *SDO* clearly dominates on longer time scales. The vertical bar has a length ±3.07 km/s and characterizes the geocentric motion of the spacecraft. The clean signal of the orbital motion establishes the stability and precision of the EVE centroid measurements, at least for this bright line. From the amplitude of the scatter we can see that the RMS variation of one 10-s integration is of order 1 km/s.

placement is relative to a source at disk center (or for a symmetrically arranged diffuse source, such as an ideal spherically-symmetric corona), rather than to an absolute wavelength. Calibration of the rest wavelength requires separate information.

At the resolution of *EVE*/MEGS-A, another substantial source of wavelength uncertainty comes from blends. In particular for He II lines at Chianti wavelengths 30.3781 and 30.3786 nm (2:1), a prominent Si XI line at 30.33268 nm (Dere *et al.*, 1997; Dere *et al.*, 2009) lies within the instrumental width (the observed offset is 0.046 nm vs. the fitted line width of $\sigma = 0.031$ nm; see Figure 1). Clearly a variable fraction of this blended feature could mimic a varying Doppler shift of the He II line, and one would expect an independent variability of these lines because of their different conditions of formation. Quantitatively, a 10% Si contribution would displace the He line centroid by the equivalent of about 50 km/s.

3. Uncertainties and error estimation

As we have seen, the EVE/MEGS-A data have excellent stability and precision. For flare research, we would like to exploit these properties and interpret some of the transient line-centroid variations (see the following sections) in terms of the motions of solar plasma as detected via the Doppler effect. How do we understand the uncertainties in this inference? In the following we make the assumption that the fluctuations consist of random errors (i.e., the basic uncertainties due to counting statistics) plus systematic errors. The latter are variations on longer time scales and are distinguishable morphologically – Figures 2 and 3 clearly show well-resolved features superposed on essentially random fluctuations. Some of these features are solar, and some are not.

At a practical level, we use two simple methods for estimating uncertainties in fitted line parameters such as the wavelength centroid. The *time-series method* examines the histogram of parameter values for a given time series, from which a standard deviation can be calculated. On the assumption that the signal from a transient can be distinguished from the background signal, e.g., by subtraction of a background term, the time-series uncertainty can be taken from times without transient emission such as a pre-flare interval. The *goodness-of-fit method* uses the deviation from the model (the standard six-parameter fit described above) as an uncertainty. Both methods will reflect the basic photon statistics, but the model fit also reflects the mathematical inadequacy of the fitting function (e.g., the hypothesis of a single line when a blend is also present). We compare these two methods for a 20-minute interval of quiet time from 12 June 2011 in Figure 4. The goodness-of-fit method method saturates as more and more data are included, presumably at the point at which the model errors outweigh counting statistics. The time-series method continues to improve, but of course if a transient (a non-random fluctuation) took place, this curve would deviate from its basic $1/\sqrt{N}$ behavior.

In the discussion below, we adopt the goodness-of-fit method for computing the uncertainty, on the grounds that it is larger and therefore more conservative. We see no problems with greatly improving the fits by going beyond our one-component Gaussian model, and we expect that this will be very useful in the deconvolution of line blends because of the excellent signal-to-noise ratio in these data.

For flares (or other transients) one can consider subtracting a background level to obtain line fits that pertain only to the flare itself. This is the approach we take below. We note, however, that this may not be exact, especially for a strong background line such as He II 30.4 nm. The problem is that the source of the transient may actually also have been a source of the solar background emission. For example, one can imagine an active-region filament contributing to the He flux, and then participating in the flare evolution. Bornmann (1990) discusses this problem (correlated background variation) in the context of *GOES* soft X-ray observations. In the analysis below we do not consider this effect, but it appears likely that simultaneous AIA observations can clarify this issue in specific cases.

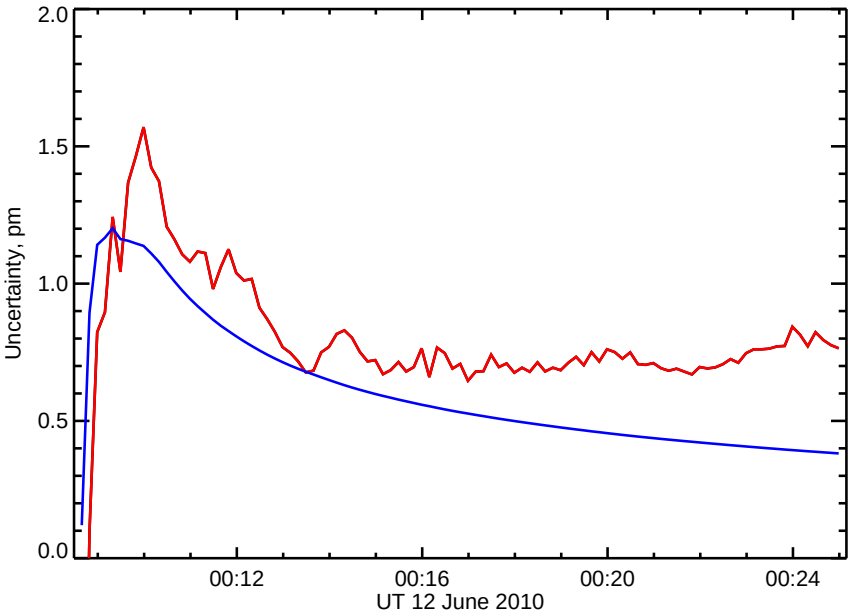

Figure 4. Uncertainty estimates for the He II 30.4 nm line centroid for a quiet 20-minute period in June 2010. The upper curve is the error reported for the cumulative Gaussian fits (the *goodness-of-fit method*, see text); the lower one is that derived from the scatter of the fit centroids (the *time-series method*).

4. Flare observations

4.1. The He line in a γ-ray flare

We are particularly interested initially in the impulsive phase of a flare, since this may correspond to a sharp transient in EVE data. The γ-ray flare SOL2010-06-12T00:53 (M2.2) had a well-defined impulsive phase (Martínez Oliveros *et al.*, 2011), and we use this as a first example. We subtract pre-flare spectra to isolate the evolving flare spectra. Figure 5 compares the hard X-ray and He II 30.4 nm light curves, showing that in this case the EUV line emission started slightly earlier than the hard X-rays, exhibited a slightly delayed impulsive-phase peak, and the decayed gradually. To observe the time variation of the line centroid, we perform the same simple Gaussian fits described above, but now on the flare excess spectra. We establish integration intervals for the preflare background, the impulsive phase, and the gradual phase as defined in Table 1; these intervals are based on the appearance of the RHESSI, GOES, and EVE light curves. The redshift results do not depend sensitively on the exact boundaries of these intervals. Figure 6 shows the time variation of the fit parameters (irradiance and line centroid).

The quiet Sun dominates the spectral irradiance in the region of the He II line, but if we make a simple time-wise background subtraction we can isolate

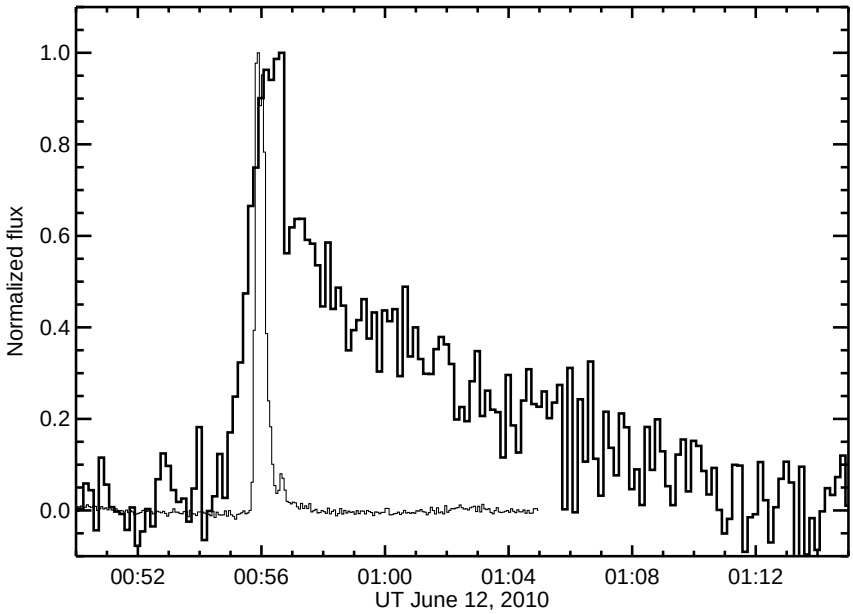

Figure 5. Comparison of EVE 30.4 nm spectral irradiance (heavy curve) with RHESSI 100-200 keV flux (light curve), after background subtraction and normalization.

the flare region specifically, with the caveat regarding correlated background described above (Bornmann, 1990) for *GOES*. This problem generally applies to observations without spatial resolution: we do not know, without reference to images, whether or not a flare brightening has altered the structure emitting the background source. For example, in He II, one can readily imagine substantial emission from a filament that then erupts and disappears at these wavelengths as the flare develops. Its pre-flare contribution, with a simple time-series subtraction, would then not be present during the flare and we would underestimate the flare flux.

Low-excitation EUV lines exhibit redshifts during the impulsive phase (Del Zanna *et al.*, 2006), consistent with the concept of momentum conservation in the evaporation flow (Canfield *et al.*, 1987). Although EVE cannot resolve the individual sources of this redshift, its precision compares favorably with (and the shift has the same sign as) the Doppler shift reported by Milligan and Dennis (2009), of 21±12 km/s, for the 25.6 nm line of He II. Their observation is of the C-class flare SOL2007-12-14 and uses EIS image-resolved spectroscopy. Table 1 gives single-component Gaussian fits for the 30.4 nm line and line excess in the preflare, impulsive, and gradual phases of the event we report. For the impulsive and gradual phases, the excess spectra give apparent Doppler shifts of 48.8±2.4 and 32.1±5.3 km/s, respectively. Since these centroid shifts are determined relative to the line as it is formed in the quiet Sun, the absolute numbers have no immediate useful interpretation. However we suggest that the difference between the impulsive-phase and gradual-phase signals, since they

Table 1. 30.4 nm Line Fits

Flare Phase	Time range	Irradiance mW/m^2	Centroid nm	Width nm	Redshift km/s
Preflare	00:50:09-00:54:29	4.26	30.3751	0.0312	
Impulsive	00:55:59-00:56:49	4.45	30.3754	0.0313	
Gradual	00:56:59-00:58:09	4.40	30.3753	0.0312	
Impulsive excess		0.197	30.3801	0.0322	48.88±2.49[a]
Gradual excess		0.137	30.3784	0.0305	32.05±5.33[a]
Impulsive-gradual					16.8±5.9[a]

[a]Statistical uncertainty

originate from sources at almost the same location, does reflect the mean Doppler motion in the flare footpoints. If so, we find a line-of-sight redward motion of 16.8 ± 5.9 km/s, which implies a downward motion of the plasma emitting in He II. This measurement compares the impulsive phase with the gradual phase of the flare, rather to the line at rest wavelength. The flare location at N22W45 suggests the possibility of a substantial projection correction for this number, so it should not be taken literally as a measurement of the vertical motion of the plasma. Because we have subtracted the non-flare background and simply intercompare the impulsive and gradual phases of the flare, this result confirms the existence of a redshift for He II lines in the impulsive phase (Canfield *et al.*, 1987). EVE proves able to determine this redshift precisely with 10 s time resolution in a flare of this magnitude. The analysis in this paper must end here; any more quantitative interpretation of this result would require analysis of line blends, notably in this case Si XI in the blue wing, as well as modeling based on geometry derived (for example) from AIA images.

On this basis of this observation we believe that the MEGS-A data may be useable to study mass motions in the footpoint regions of a flare statistically, with appropriate analysis and modeling, in spite of their Sun-as-a-star character and systematic uncertainties. The statistical error bars in velocity for this M2 event compare favorably with those of Del Zanna *et al.* (2006) for an M1 event (a general 10 km/s uncertainty estimate) and Milligan and Dennis (2009) for a C1.1 flare (±12 km/s for He II), using CDS and EIS respectively. The actual derived velocities from EVE should be viewed with caution until we have observed further events and carried out a more complete analysis for spectral line blends.

4.2. Other flares, other lines

EVE also has measures Doppler signatures in high-temperature coronal emission lines, where the problem of correlated background does not apply since these lines do not appear in the background (quiet-Sun) spectra. We show the EVE data for the Fe XXIV line at 19.20285 nm, known for flare contributions to the EIT 195Å and similar images, for four flares, in Figure 7. The events shown are the only two γ-ray flares (both M-class) and the only two X-class events in the

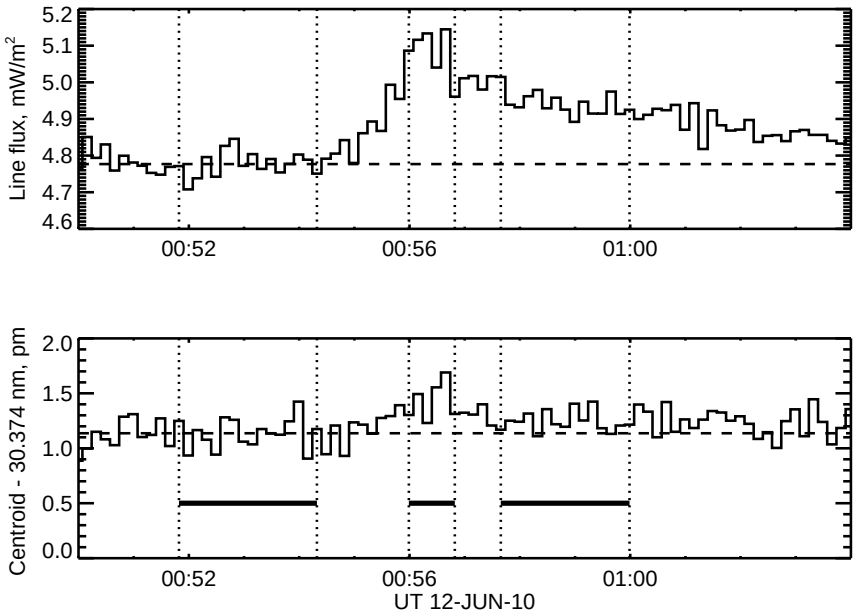

Figure 6. Results of Gaussian fits to the 30.4 nm line observed by EVE. *Upper:* peak irradiance; *lower:* centroid. The horizontal lines show the time intervals for the background, impulsive-phase, and gradual-phase integrations for the values given in Table 1.

Table 2. Four flares observed in Fe XXIV emission

IAU identifier	*GOES* class	Background[a]	Location	Shift (pm)
SOL2010-06-12T00:53	M2.0	00:45	N23W43	−2.8
SOL2011-02-24T07:35	M3.5	07:30	N16E87[b]	−24
SOL2011-02-15T01:56	X2.2	01:45	S20E12[b]	−1.3
SOL2011-03-09T23:23	X1.5	23:17	N08W09	+1.0

[a]Start times of 50-s intervals.
[b]Positions from the RHESSI flare catalog; otherwise NOAA.

EVE record at time of writing. We use the same standard fitting procedure as before.

For each of the flares in Table 2 we have used the standard Gaussian fitting to characterize the centroid of the Fe XXIV line at 19.20285 nm, and show the results in Figure 8. The observed centroid wavelengths do not match the Chianti values but the scatter (of order 0.01 nm) is consistent with expectations from the EVE wavelength calibration, i.e. a small fraction of the spectral resolution. The precision of the observations is comparable to the error component predicted by Equation 1, and so it is likely that this can be effectively removed in future studies. The precision of the data suggests that this may lead to the characterization of more subtle effects, such as abundance variations or DEM properties.

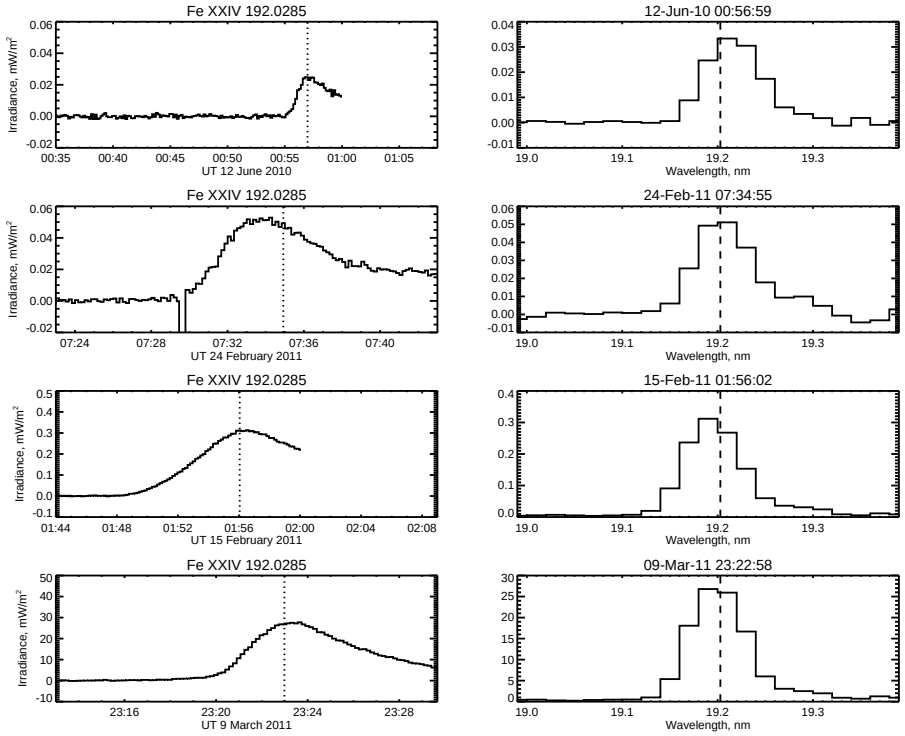

Figure 7. Fits to the Fe XXIV line at 19.20285 nm for four flares (see Table 2). Each pair of plots is the time series of the line irradiance, with the dotted line showing *GOES* maximum, and the spectrum at that time. For each plot an averaged background irradiance or spectrum has been subtracted. The two events at the bottom are the *SDO* X-class events of this cycle, at time of writing, and we note that SOL2011-03-09 flare was especially bright in Fe XXIV emission.

The centroids of the Fe XXIV line fits show some scatter for the M-class flares, but are relatively well defined for the X-class flares, and in each case show a trend of centroid displacement is to the redward as the flare progresses. This is qualitatively consistent with the diminishing blueshifts expected from chromospheric evaporation. The inferred velocities are smaller than typical spatially-resolved quantities (e.g., Del Zanna *et al.*, 2006), but that is consistent with the dilution of the signal from the mixing of different image elements. As the flares progress, the blue-shifted footpoint sources become swamped by the coronal loop emission, which is near the rest wavelength.

5. Conclusions

The EVE data have taken a major step in defining the EUV spectrum associated with the impulsive phase of a solar flare. In this paper we have outlined the capability of EVE/MEGS-A for Doppler measurements, and have shown that the Level-2 data have excellent stability and precision, with the line centroid of He II 30.4 nm determined to well below 1 pm in terms of random error.

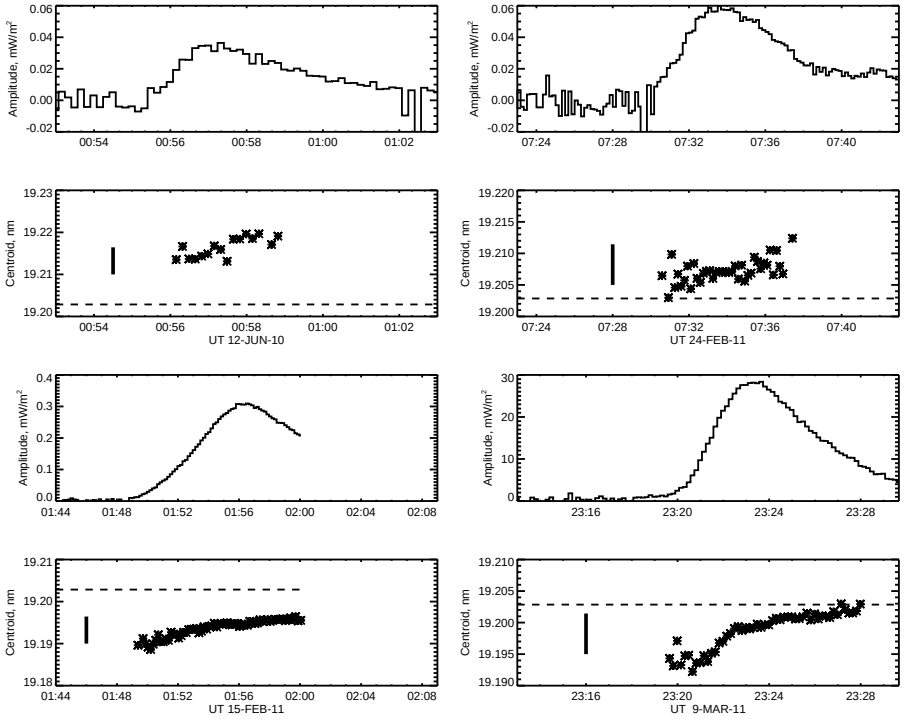

Figure 8. Results of Gaussian fits for the Fe XXIV line at 19.20285 nm, in the four chosen flares. In each case the dashed line on the redshift panel represents the Chianti wavelength of the line. The heavy vertical bars show 100 km/s.

We have studied some aspects of these data for the impulsive phase of a particularly interesting event, the white-light and γ-ray flare SOL2010-06-12T00:57 (M2.0), with the conclusion that the impulsive-phase emission shows a redshift consistent with earlier observations of other flares (Del Zanna *et al.*, 2006, Milligan and Dennis, 2009), and for the blended He II line at 25.6 nm by Del Zanna *et al.* (2011), but with smaller uncertainties. Because this line is complicated we do not attempt to draw quantitative conclusions here, but expect that due reference to simultaneous imaging and modeling will make these data extremely useful for studying flare dynamics. EVE also readily reveals Doppler signatures for optically-thin lines such as Fe XXIV line at 19.20285 nm. These are consistent with our current knowledge of flare physics. We expect a great deal from the different perspective offered by EVE, with its many dozens of emission lines, when combined with image information and numerical modeling. This will especially be true for the major flares, for which the EVE data have excellent precision and complete time-series characterization, and so we encourage studies that take advantage of these properties.

Acknowledgements: This work was supported by NASA via Contract NAS5-98033 for *RHESSI*. Authors Fletcher and Hudson thank the International Space

Science Institute (Bern) for support. This work was supported by the EU's SOLAIRE Research and Training Network at the University of Glasgow (MTRN-CT-2006-035484), Rolling Grant ST/F002637/1 and ST/1001808/1 from the UKs Science and Technology Facilities Council, and Leverhulme Foundation Grant F00-179A.

References

Allred, J.C., Hawley, S.L., Abbett, W.P., Carlsson, M.: 2005, *Astrophys. J.* **630**, 573. doi:10.1086/431751.

Bornmann, P.L.: 1990, *Astrophys. J.* **356**, 733. doi:10.1086/168880.

Canfield, R.C., Metcalf, T.R., Strong, K.T., Zarro, D.M.: 1987, *Nature* **326**, 165. doi:10.1038/326165a0.

Cheng, C., Tandberg-Hanssen, E., Bruner, E.C., Orwig, L., Frost, K.J., Kenny, P.J., Woodgate, B.E., Shine, R.A.: 1981, *Astrophys. J. (Lett.)* **248**, L39. doi:10.1086/183619.

Crotser, D.A., Woods, T.N., Eparvier, F.G., Triplett, M.A., Woodraska, D.L.: 2007, In: *Society of Photo-Optical Instrumentation Engineers (SPIE) Conference Series*, *Presented at the Society of Photo-Optical Instrumentation Engineers (SPIE) Conference* **6689**. doi:10.1117/12.732592.

Del Zanna, G., Berlicki, A., Schmieder, B., Mason, H.E.: 2006, *Solar Phys.* **234**, 95. doi:10.1007/s11207-006-0016-6.

Del Zanna, G., Mitra-Kraev, U., Bradshaw, S.J., Mason, H.E., Asai, A.: 2011, *Astron. Astrophys.* **526**, A1. doi:10.1051/0004-6361/201014906.

Dere, K.P., Landi, E., Mason, H.E., Monsignori Fossi, B.C., Young, P.R.: 1997, *Astron. Astrophys. Suppl.* **125**, 149. doi:10.1051/aas:1997368.

Dere, K.P., Landi, E., Young, P.R., Del Zanna, G., Landini, M., Mason, H.E.: 2009, *Astron. Astrophys.* **498**, 915. doi:10.1051/0004-6361/200911712.

Didkovsky, L., Judge, D., Wieman, S., Woods, T., Jones, A.: 2009, *Solar Phys.*, 182. doi:10.1007/s11207-009-9485-8.

Emslie, A.G., Dennis, B.R., Holman, G.D., Hudson, H.S.: 2005, *Journal of Geophysical Research (Space Physics)* **110**, 11103. doi:10.1029/2005JA011305.

Feldman, U.: 1987, *Atlas of extreme ultraviolet spectroheliograms from 170 to 625 A. Volume 1; Volume 2.*

Lemaire, P., Gouttebroze, P., Vial, J., Curdt, W., Schühle, U., Wilhelm, K.: 2004, *Astron. Astrophys.* **418**, 737. doi:10.1051/0004-6361:20034405.

Martínez Oliveros, J.C., Couvidat, S., Schou, J., Krucker, S., Lindsey, C., Hudson, H.S., Scherrer, P.: 2011, *Solar Phys.*, 7. doi:10.1007/s11207-010-9696-z.

Milligan, R.O., Dennis, B.R.: 2009, *Astrophys. J.* **699**, 968. doi:10.1088/0004-637X/699/2/968.

Raymond, J.C., Holman, G., Ciaravella, A., Panasyuk, A., Ko, Y., Kohl, J.: 2007, *Astrophys. J.* **659**, 750. doi:10.1086/512604.

Woodgate, B.E., Brandt, J.C., Kalet, M.W., Kenny, P.J., Tandberg-Hanssen, E.A., Bruner, E.C., Beckers, J.M., Henze, W., Knox, E.D., Hyder, C.L.: 1980, *Solar Phys.* **65**, 73. doi:10.1007/BF00151385.

Woods, T.N., Eparvier, F.G., Fontenla, J., Harder, J., Kopp, G., McClintock, W.E., Rottman, G., Smiley, B., Snow, M.: 2004, *Geophys. Res. Lett.* **31**, 10802. doi:10.1029/2004GL019571.

Woods, T.N., Eparvier, F.G., Hock, R., Jones, A.R., Woodraska, D., Judge, D., Didkovsky, L., Lean, J., Mariska, J., Warren, H., McMullin, D., Chamberlin, P., Berthiaume, G., Bailey, S., Fuller-Rowell, T., Sojka, J., Tobiska, W.K., Viereck, R.: 2010, *Solar Phys.*, 3. doi:10.1007/s11207-009-9487-6.